

## Material Science and Engineering with Advanced Research

# Proximity-induced Ferromagnetic Order in Graphene on Transition Metal Dichalcogenides

Partha Goswami\*

Deshbandhu College, University of Delhi

**\*Corresponding author:** Partha Goswami, Deshbandhu College, University of Delhi, Kalkaji, New Delhi-110019, India; E-mail: physicsgoswami@gmail.com

**Article Type:** Mini Research, **Submission Date:** 04 November 2015, **Accepted Date:** 11 December 2015, **Published Date:** 29 January 2016.

**Citation:** Partha Goswami (2016) Proximity-induced Ferromagnetic Order in Graphene on Transition Metal Dichalcogenides. Mater. Sci. Eng. Adv. Res 1(3): 18-21. doi: <https://doi.org/10.24218/msear.2015.14>.

**Copyright:** © 2016 Partha Goswami. This is an open-access article distributed under the terms of the Creative Commons Attribution License, which permits unrestricted use, distribution, and reproduction in any medium, provided the original author and source are credited.

### Abstract

We start with a graphene (GTMD) monolayer on two dimensional transition metal dichalcogenides (such as,  $\text{MoS}_2/\text{MoSe}_2/\text{WS}_2/\text{WSe}_2$ ) Hamiltonian ( $H_G$ ) which is built on the orbital Hamiltonian ( $H_0$ ) for pristine graphene. The former, apart from  $H_0$ , comprises of the staggered potential term ( $H_\Delta$ ) describing the effective orbital energy difference on A and B sub-lattices of graphene, the sub-lattice-resolved intrinsic spin-orbit coupling ( $H_{\text{SO}}$ )— a next-nearest neighbor hopping much larger than that in the hydrogenated graphene, the pseudo-spin inversion asymmetry related spin-orbit coupling term— a next-nearest neighbor hopping with the spin-flip, and the Rashba-type spin-orbit coupling ( $\lambda'_R$ ) which is actually the nearest-neighbor spin-flip hopping. The pen-ultimate term takes care of the spin-splitting away from the Dirac points K and K'. The term  $H_G$  is basically a low-energy effective Hamiltonian around K and K' in the basis ( $A_\uparrow, B_\downarrow, A_\downarrow, B_\uparrow$ ) in momentum space. We calculate the electronic band dispersion of GTMD exchange coupled to the magnetic impurities, such as Fe atoms deposited to the graphene surface. The presence of the giant spin-orbit coupling fields give rise to large spin-polarization and inverted band structure (see Figure1). The inverted band structure is a precursor of the quantum spin Hall effect. We find that the band inversion feature is robust against the proximity-induced ferromagnetic order.

**Keywords:** Pristine graphene, Transition metal dichalcogenides, Sub-lattice-resolved intrinsic spin-orbit coupling, Pseudo-spin inversion asymmetry related spin-orbit coupling term, Rashba-type spin-orbit coupling.

**PACS:** 73.22.-f, 61.48.Gh, 71.15.Mb

### Main Text

In this short letter, we study the magnetic impurity effects in a graphene (GTMD) monolayer on two dimensional transition metal dichalcogenides (such as,  $\text{MoS}_2/\text{MoSe}_2/\text{WS}_2/\text{WSe}_2$ ). Since its first successful isolation in 2004 [1], graphene has attracted immense attention as it was found to possess host of unusual properties, such as the large in-plane stiffness [2], the high carrier mobility, the low resistivity, the larger (than metal)

optical absorption at the Plasmon-resonance (PR) [3], the PR wavelength tunability by an electric gate voltage [4,5], and so on. Though the first among the properties listed leads to a relatively high longitudinal optical zone-boundary phonon energies (~160 meV) [6], the second and the third listings are the outcomes of the relatively weak scattering due to the longitudinal acoustic phonons [7,8] dominant around and below room temperature. These two properties also allow quantum Hall measurements even at room temperature and make graphene seemingly useful as a substitute of silicon in transistors. Despite these remarkable possibilities, it has not been possible to fully exploit the graphene's potential due to the difficulty of opening a sizable insulating gap in its band structure. As a result, attention had begun to shift to other two-dimensional (2D) systems such as silicene [9], phosphorene [10], TMDCs [11,12] like molybdenum disulfide ( $\text{MoS}_2$ ), tungsten diselenide ( $\text{WSe}_2$ ), etc.. Though the ridged structure of silicene allow creation of a tunable band-gap, but like graphene'silicene' would be a much faster conductor of electrons than most TMDCs. Besides, a 2D sheet of silicene would be highly reactive and completely unstable in air and thus proved to be a poor fit for digital electronics. As regards phosphorene, unlike graphene, it has a natural band gap — and it is more stable than silicene. However, phosphorene also conducts electrons very swiftly. The investigations of the Andras Kis's team [13] showed that a single layer of TMDCs can capture more than 10% of incoming photons, and this process can also be reversed to turn electricity into light. This extra-ordinary ability makes TMDCs promising candidates for applications in quantum cryptography and communications. Side-by-side this search for the new 2D materials, the suggestion has been to combine them with known 2D materials in such a way that all their different advantages are properly utilized. The appropriate integration of different layers of two-dimensional materials could have very interesting properties and, consequently, much wider applications than previously thought. For example, very photosensitive TMDC and optically transparent and conductive graphene could collectively create a very efficient photovoltaic device. Ideally, in fact, every heterostructure could be utilized for creating novel, multifunctional devices.

The low-energy dimensionless Hamiltonian [14] for a graphene sheet on TMDC (such as, MoS<sub>2</sub>/MoSe<sub>2</sub>/WS<sub>2</sub>/WSe<sub>2</sub>) around Dirac point K and K' in the basis (a<sub>K↑</sub>, b<sub>K↓</sub>, a<sub>K↓</sub>, b<sub>K↑</sub>) in momentum space may be written down explicitly as

~ 24 μeV). The parameter λ<sub>R</sub> = λ'<sub>R</sub> / (ħv<sub>F</sub>/a) is the extrinsic Rashba spin-orbit coupling (RSOC), that allow for external tuning of the band gap in GTMDC and connects the nearest neighbours with spin-flip. It, thus, arises because the inversion symmetry is

$$H/\left(\frac{\hbar v_F}{a}\right) = \sum_{\delta k} (a^\dagger_{\delta k \uparrow} b^\dagger_{\delta k \downarrow} a^\dagger_{\delta k \downarrow} b^\dagger_{\delta k \uparrow}) \frac{\mathbb{H}((\delta k))}{\left(\frac{\hbar v_F}{a}\right)} \begin{pmatrix} a_{\delta k \uparrow} \\ b_{\delta k \downarrow} \\ a_{\delta k \downarrow} \\ b_{\delta k \uparrow} \end{pmatrix} \quad (1)$$

$$\frac{\mathbb{H}(\delta k)}{\left(\frac{\hbar v_F}{a}\right)} = \begin{pmatrix} \Delta + M + \xi \Delta_{soc}^A & h_+^\xi & -(\lambda^+ + \lambda^-)i\delta k_- & -a\delta k_+^\xi \\ h_+^{\xi*} & -\Delta - M - \xi \Delta_{soc}^B & -a\delta k_-^\xi & -(\lambda^+ - \lambda^-)i\delta k_+ \\ (\lambda^+ + \lambda^-)i\delta k_+ & -a\delta k_+^\xi & \Delta - M - \xi \Delta_{soc}^A & h_-^\xi \\ -a\delta k_-^\xi & (\lambda^+ - \lambda^-)i\delta k_- & h_-^{\xi*} & -\Delta + M + \xi \Delta_{soc}^B \end{pmatrix} \quad (2)$$

$$h_+^\xi = \frac{3}{2} i \lambda_R (E)(1 + \xi), \quad h_-^\xi = \frac{3}{2} i \lambda_R (E)(1 - \xi) \quad (3)$$

Here the nearest neighbor hopping is parameterized by a hybridization  $t$  ( $(\hbar v_F)/a$ ) =  $(\sqrt{3}/2)t$ ,  $a = 2.46 \text{ \AA}$  is the pristine graphene lattice constant. Also,  $\delta k_\pm^\xi \rightarrow \delta k_\pm$  (that is,  $\delta k_x \pm i\delta k_y$  for the Dirac point K ( $\xi = +1$ ) and  $\delta k_\pm^\xi \rightarrow \delta k_\pm^*$  (that is,  $\delta k_x \pm i\delta k_y$ ) for the Dirac point K' ( $\xi = -1$ ). The quantity  $E(s_z, t_z) = \xi t' s_z t_z + \Delta t_z + M s_z$ , with the spin index  $s_z = \pm 1$  and the sub-lattice pseudo-spin index  $t_z = \pm 1$ . The parameters orbital proximity gap the intrinsic parameters  $\Delta_{soc}^A$  and  $\Delta_{soc}^B$ , and the extrinsic Rashba parameter  $t_R$  ( $E_z$ ) allow for tuning by the applied electric field. Since the MoS<sub>2</sub> layer provides different environment to atoms A and B in the graphene-cell, there is this dimension-less orbital proximity gap  $\Delta = \Delta_{Orbital}/((\hbar v_F)/a)$  arising from the effective staggered potential induced by the pseudo-spin symmetry breaking. The orbital gap  $\Delta_{Orbital}$  is about 0.5 meV [14] in the absence of electric field. When the field crosses a limiting value 0.5 V/nm, the gap exhibits a sharp increase. This gap is related to the transfer of the electronic charge from graphene to MoS<sub>2</sub>. The quantum anomalous Hall state could be accessed in graphene on TMDC by introducing an exchange field. The crucial term, viz. the exchange field  $M'$  ( $M = M'/((\hbar v_F)/a)$ ) arises due to proximity coupling to a ferro-magnet such as depositing Fe atoms (time-reversal breaking impurities) to the graphene surface. Due to the hybridization of the carbon orbitals with the d-orbitals of Mo/W, there is the sub-lattice-resolved, giant intrinsic spin-orbit couplings ( $t_{so}^A, t_{so}^B$ ) ( $\Delta_{soc}^A = (t_{so}^A)/((\hbar v_F)/a)$ ) and  $\Delta_{soc}^B = (t_{so}^B)/((\hbar v_F)/a)$ ). These couplings correspond to next-nearest neighbor hopping [15] without spin-flip. The spin-orbit field parameters for GTMDC are about 0.50 meV, which is 20 times more than that in pure graphene [16] ( $t_{soc}$

broken when graphene is placed on top of a TMDC. While the intrinsic parameters  $\Delta_{soc}$  and  $\Delta_{soc}$  change rather moderately with the increase in the applied electric field, the Rashba parameter  $\lambda_R$  almost doubles in increasing the field from -2 to 2 V/nm. For the pristine graphene  $\lambda'_R \approx 10 \text{ meV}$  whereas for GTMDC (WSe<sub>2</sub>) it is 0.56 meV. Wang et al. [17], however, have reported it to be approximately 1 meV. The spin-splitting by the Rashba term away from the points K and K' is the same as that at K and K'. The three spin-orbit interaction terms, with coupling constant ( $t_{so}^A, t_{so}^B$ ) and  $\lambda'_R$ , are induced by interfacial interactions. The all four substrate-induced interaction terms,  $\Delta_{Orbital}$ , ( $t_{so}^A, t_{so}^B$ ) and  $\lambda'_R$ , are time-reversal invariant and absent by inversion symmetry in isolated graphene sheets. The pseudo-spin inversion asymmetry (PIA) driven spin-orbit coupling term, on the other hand, represents the next-nearest-neighbor, unlike the Rashba term, same sub-lattice hopping away from K and K' albeit with a spin flip. In the basis ( $a_{K\uparrow}, b_{K\downarrow}, a_{K\downarrow}, b_{K\uparrow}$ ), the PIA driven terms, involving  $\lambda^+ = \lambda^+ / ((\hbar v_F)/a)$  and  $\lambda^- = \lambda^- / ((\hbar v_F)/a)$ , could be written in a manner as shown in Eq. (2). Here  $\lambda^+, \lambda^-$  respectively, are the spin-orbit interactions representing the average coupling, and the differential coupling between the A and B sub-lattices. The values of the orbital and spin-orbital parameters are summarized in Table. These parameters can be tuned by a transverse electric field and vertical strain. Only in the case of graphene on WSe<sub>2</sub> the orbital gap is smaller than the magnitudes of the intrinsic spin-orbit coupling parameters. This is a signature of the inverted band structure as seen in Figure 1 and Table.

The energy eigen-values ( $E(a|\delta k|)$ ) of the matrix (2) are given by

TMDC	T [eV]	v <sub>F</sub> [m/s]	Δ <sub>Orbital</sub> [meV]	t <sub>so</sub> <sup>A</sup> [meV]	t <sub>so</sub> <sup>B</sup> [meV]	λ' <sub>R</sub> [meV]	λ <sup>+</sup> [meV]	λ <sup>-</sup> [meV]	ΔE <sub>v</sub> [eV]	ΔE <sub>c</sub> [eV]
WSe <sub>2</sub>	2.51	8.16	0.54	-1.22	1.16	0.56	-5.23	-0.15	0.22	1.15
WS <sub>2</sub>	2.66	8.46	1.31	-1.02	1.21	0.36	-4.79	2.83	1.13	0.30
MoSe <sub>2</sub>	2.53	8.22	0.44	-0.19	0.16	0.26	5.98	-1.06	0.56	0.92
MoS <sub>2</sub>	2.67	8.51	0.52	-0.23	0.28	0.13	-3.45	1.01	1.51	0.04

a quartic. In terms of the powers of  $\epsilon$  ( where  $\epsilon \equiv E(a|\delta k|)/\lambda_R$ ), in the absence of PIA driven terms, the quartic may be written as

$$\epsilon^4 - 2 \epsilon^2 b - 4 \epsilon a + c = 0, \tag{4}$$

where

$$b(|\delta k|) = \left[ \left( \frac{\Delta}{\lambda_R} \right)^2 + \left( \frac{M}{\lambda_R} \right)^2 + \left( \left( \frac{\Delta^A_{soc}}{\lambda_R^2} \right)^2 + \left( \frac{\Delta^B_{soc}}{\lambda_R^2} \right)^2 \right) / 2 + (1 + \xi^2) + \left( \frac{(\alpha|\delta k|)^2}{\lambda_R^2} \right) \right. \\ \left. - \xi \left\{ \left( \frac{\Delta^B_{soc}}{\lambda_R} \right) + \left| \left( \frac{\Delta^A_{soc}}{\lambda_R} \right) \right| \right\} \left( \frac{M}{\lambda_R} \right) \right], \\ a(|\delta k|) = \left\{ \left( \frac{\Delta^B_{soc}}{\lambda_R} \right) - \left| \left( \frac{\Delta^A_{soc}}{\lambda_R} \right) \right| \right\} \left[ 1 - \left( \frac{\Delta}{2\lambda_R} \right) \left\{ \left( \frac{\Delta^B_{soc}}{\lambda_R} \right) + \left| \left( \frac{\Delta^A_{soc}}{\lambda_R} \right) \right| \right\} + \xi \left( \frac{\Delta}{\lambda_R} \right) \left( \frac{M}{\lambda_R} \right) \right], c(|\delta k|) = \sum_{j=1}^5 c_j, \\ c_1 = \left\{ \left( \frac{\Delta}{\lambda_R} \right)^2 - \left( \frac{M}{\lambda_R} \right) - \xi \left( \frac{\Delta^B_{soc}}{\lambda_R} \right) \right\}^2 \times \left\{ \left( \frac{\Delta}{\lambda_R} \right)^2 - \left( \frac{M}{\lambda_R} \right) - \xi \left| \left( \frac{\Delta^A_{soc}}{\lambda_R} \right) \right| \right\}^2, \\ c_2 = (1 + \xi)^2 \left[ \left\{ \left( \frac{\Delta}{\lambda_R} \right) - \left( \frac{M}{\lambda_R} \right) \right\}^2 + \xi \left\{ \left( \frac{\Delta^B_{soc}}{\lambda_R} \right) + \left| \left( \frac{\Delta^A_{soc}}{\lambda_R} \right) \right| \right\} \left\{ \left( \frac{\Delta}{\lambda_R} \right) - \left( \frac{M}{\lambda_R} \right) \right\} + \left( \frac{\Delta^B_{soc}}{\lambda_R} \right) \left| \left( \frac{\Delta^A_{soc}}{\lambda_R} \right) \right| \right], \\ c_3 = (1 - \xi)^2 \left[ \left\{ \left( \frac{\Delta}{\lambda_R} \right) + \left( \frac{M}{\lambda_R} \right) \right\}^2 - \xi \left\{ \left( \frac{\Delta^B_{soc}}{\lambda_R} \right) + \left| \left( \frac{\Delta^A_{soc}}{\lambda_R} \right) \right| \right\} \left\{ \left( \frac{\Delta}{\lambda_R} \right) + \left( \frac{M}{\lambda_R} \right) \right\} + \left( \frac{\Delta^B_{soc}}{\lambda_R} \right) \left| \left( \frac{\Delta^A_{soc}}{\lambda_R} \right) \right| \right], \\ c_4 = \left( \frac{2(\alpha|\delta k|)^2}{\lambda_R^2} \right) \left[ \left\{ \left( \frac{\Delta}{\lambda_R} \right)^2 - \left( \frac{M}{\lambda_R} \right) \right\}^2 + \xi \left\{ \left( \frac{\Delta^B_{soc}}{\lambda_R} \right) + \left| \left( \frac{\Delta^A_{soc}}{\lambda_R} \right) \right| \right\} \left( \frac{M}{\lambda_R} \right) - \left( \frac{\Delta^B_{soc}}{\lambda_R} \right) \left| \left( \frac{\Delta^A_{soc}}{\lambda_R} \right) \right| \right], c_5 = \left( \frac{(\alpha|\delta k|)^4}{\lambda_R^4} \right). \tag{5}$$

The table above shows that  $(\Delta^B_{soc})/\lambda_R \approx |(\Delta^A_{soc})/\lambda_R|$  in all the cases of MoS<sub>2</sub>, MoSe<sub>2</sub>, WS<sub>2</sub>, and WSe<sub>2</sub>. As a result, in the equation  $\epsilon^4 - 2 \epsilon^2 b - 4 \epsilon a + c = 0$ , the term  $(4 \epsilon a)$  could be ignored compared to the other terms. Thus,  $\epsilon^2 \approx b + s \sqrt{(b^2 - d)}$  or,

$$\epsilon_{s,\mu}(|\delta k|) = \mu \sqrt{b(|\delta k|) + s \sqrt{(b(|\delta k|)^2 - c(|\delta k|))}}. \tag{6}$$

The simplified single particle excitation spectrum in (6) may be used for calculating the thermodynamic, optical, transport properties, and so on. Our graphs in Figure 1 shows that the graphene on WSe<sub>2</sub> possesses the inverted Dirac bands (see

Figure 1(a)), due to the strong (100 times stronger than in pristine graphene) spin-orbit coupling. Obviously, it can act as a quantum spin Hall insulator. In bulk, however, graphene on monolayer WSe<sub>2</sub> experiences a gap, making it an insulator. We

find the band inversion feature is robust against the magnetic impurities (see Figure 1 (b)) depositing Fe atoms to the graphene surface. We have also found that the inversion is robust against an applied transverse electric field and vertical strain. The latter effects will be reported in a future communication.

It is easy to see that when only the Rashba coupling and the exchange field are present, the energy band is given by the spectrum obtained by MacDonald et al. [17,18]. This provides us a verification of the correctness of our result derived in (5).

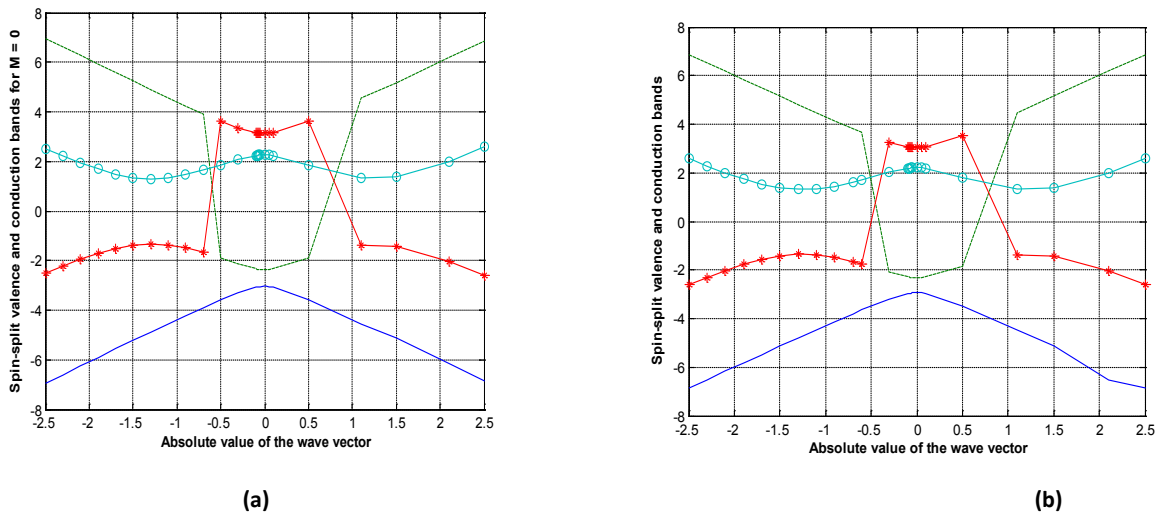


**Figure 1:** The plots of spin-split valence and conduction bands as a function of the absolute value of the wave vector in the case of graphene on WSe<sub>2</sub>. While in (a), M=0, it is non-zero for (b). The essential features are (i) opening of an orbital gap due to the effective staggered potential, (ii) the anti-crossing of the bands due to the intrinsic spin-orbit coupling, and (iii) spin splittings of the bands due to spin-orbit coupling and breaking of the space inversion symmetry. The exchange field M' (we have taken M' = λ<sub>R</sub>'/10) arises due to proximity coupling to a ferro-magnet such as depositing Fe atoms (time-reversal breaking impurities) to the graphene surface

Our continuum model, the one including the effective Rashba SO coupling and the exchange field  $M$  only, have the same form as that in Eq.(1) of ref.17. These authors have calculated the transverse anomalous Hall conductivity of their system subsequently, given by  $S_{xy} = (e^2/h)C$ , with  $C$  as the Chern number of all occupied bands that can be obtained as the usual  $k$ -space integral [17]. The integrand,  $U(k)$ , is the so-called Berry curvature of all states below the Fermi level. The function  $U(k)$  plays a role of an effective magnetic field in the  $k$ -space. Our preliminary investigation with the TMDC suggests that the topological properties of the QAHE state in graphene can be controlled by tuning the position of the Fermi level.

## References

1. Novoselov KS, Geim AK, Morozov SV, Jiang D, Zhang Y, Dubonos SV, et al. Science. 2004; 306(5696):666-669.
2. Ovid'ko IA. Rev. Adv. Mater. Sci. 2013; 34:1-11.
3. Maier SA. Plasmonics: Fundamentals and Applications. Springer; 2007.
4. Castro Neto AH, Guinea F, Peres NMR, Novoselov KS, Geim AK. Rev. Mod. Phys. 2009; 81:109–162.
5. Fei, Rodin AS, Andreev GO, Bao W, McLeod AS, Wagner M, et al. Nature. 2012; 487:82–85. doi:10.1038/nature11253.
6. Yao Z, Kane CL, Dekker C. Phys. Rev. Lett. 2000; 84:2941.
7. Hwang EH, Das Sarma S. Phys. Rev. B. 2008; 77:115449.
8. Stauber T, Peres NMR, Guinea F. Phys. Rev. B. 2007; 76:205423.
9. Geoff Brumfiel. Nature. 2013; 495:152.
10. Li L. Nature Nanotechnol. 2014; 9:372.
11. Mak KF, Lee C, Hone J, Shan J, Heinz TF. Phys. Rev. Lett. 2010; 105:136805.
12. Radisavljevic B, Radenovic A, Brivio J, Giacometti V, Kis A. Nature Nanotechnol. 2011; 6:147.
13. Gmitra M, Kochan D, Hognl P, Fabian J. 2015: arXiv: 1510.00166.
14. Kunschuh S, Gmitra M, Fabian J. Phys. Rev. B. 2010; 82:245412.
15. Gmitra M, Kunschuh S, Ertler C, Ambrosch-Draxl C, Fabian J. Phys. Rev. B. 2009; 80:235431.
16. Wang Z, Ki DK, Chen H, Berger H, MacDonald AH, Morpurgo AF. Nat. Commun. 2015; 6:8339.
17. Tse WK, Qiao Z, Yao Y, MacDonald AH, Niu Q. Phys. Rev. B. 2011; 83:155447.
18. Qiao Z, Ren W, Chen H, Bellaiche L, Zhang Z, MacDonald AH, et al. Phys. Rev. Lett. 2014; 112:116404.